PAPER

NJC
www.rsc.org/njc

Synthesis, solid-state molecular structure and solution dynamics of new alkoxy stannylene-transition metal complexes†

Michael Veith,* Markus Ehses and Volker Huch

Institute of Inorganic Chemistry, Saarland University, PO Box 15 11 50, 66041 Saarbrücken, Germany. E-mail: veith@mx.uni-saarland.de

Received (in Toulouse, France) 21st September 2004, Accepted 23rd November 2004
First published as an Advance Article on the web 14th December 2004

Reactions of the dimeric alkoxy stannylene $[Sn(O^tBu)_2]_2$ (**1**) with the THF-stabilised group 6 pentacarbonyl fragments $[M(CO)_5(THF)]$ (M = Cr, W) yield the trinuclear complexes $[\{(OC)_5M\}\{\eta^1\text{-}Sn_2(O^tBu)_2(\mu\text{-}O^tBu)_2\}]$ [M = Cr (**2a**), W (**2b**)] and tetranuclear complexes $[\{(OC)_5M\}\{(OC)_5M'\}\{\mu,\eta^{1:1}\text{-}Sn_2(O^tBu)_2(\mu\text{-}O^tBu)_2\}]$ [M = Cr, M′ = W (**3a**); M = M′ = Cr (**3b**), W (**3c**)]. The solid-state structures of **2a**, **2b**, **3a** and **3b** have been determined by X-ray crystallography: the tri- and tetranuclear complexes are isotypic and crystallise in the monoclinic space group $P2_1/n$ and $P2_1/m$, respectively. The dimeric structure of the starting molecule is retained in the complexes. Steric and electronic effects in the metal complexes can be separately assigned by correlating systematic changes in the solid-state structures with solution NMR spectra of the complexes. In the ^1H, $^{13}C\{^1H\}$ and $^{119}Sn\{^1H\}$ temperature-variable NMR spectra, strong drifts of the chemical shifts are observed. The ^1H and ^{13}C NMR spectra for the trinuclear complexes reveal two consecutive exchange mechanisms, which involve the bridging and terminal O^{t}Bu substituents. The free activation enthalpies could be determined by lineshape analysis for **2a** (low-temperature process) and **2b** (low- and high-temperature processes). The low-temperature exchange most probably occurs *via* an associative mechanism.

Introduction

The electronic and coordinative unsaturation ($\sigma^2\lambda^2$) of tin in stannylenes, the heavier congeners of carbenes, is compensated either through σ- or π-donation, steric encumbrance and/or extension of the coordination number by binding to a transition metal moiety.[6] Stannylenes show an amphiphilic behaviour towards acids,[7] bases,[8–12] and oxidants[13–18] that is attributed to the hybridisation of the electron-deficient tin centre, which is regarded as being intermediate between $(sp^2)^4(p_z)^0$ and $s^2(p_{x,y})^2(p_z)^0$.[19] Both descriptions take into account the presence of a lone pair of electrons and an empty p-orbital perpendicular to the plane formed by tin and the α-atoms of the two substituents.

Concurrently to the syntheses of the first stable stannylenes in the late 1970's, a number of remarkable papers appeared on the synthesis and characterisation of transition metal complexes with stannylenes as ligands by the groups of Marks,[20] Jutzi,[21] duMont[22] and Lappert.[23–25] Major reviews on structures and spectroscopic features of transition metal complexes with stannylene ligands have appeared in the late 80's to early 90's.[26–28] Renewed interest in these types of complexes has grown as they can provide heterobimetallic complexes or clusters,[29] stabilise stannylene complexes with low coordination number,[29] be used in the synthesis of heteroleptic stannylenes[30–32] and as single-source precursors.[33,34]

Several synthetic approaches to stannylene transition metal complexes have been applied,[26,35] of which the most convenient is the replacement of a (labile) ligand by the stannylene.

The main structural types of stannylene complexes are sketched in Fig. 1: ψ-trigonal planar coordination geometry around tin (**A**) stabilised by electron-releasing or sterically demanding substituents on tin,[24,30,31,36,37] ψ-tetrahedron (**B**) or ψ-pentagonal bipyramid (**C**).[38–40] The mesomeric effect of lone pairs of electrons on the substituents (*e.g.*, amides or alkoxides), dimerisation of the stannylene ligand {*e.g.*, $\{[L_nM]_m[Sn(O^tBu)(\mu\text{-}O^tBu)]_2\}$ [ML_n = $Ni(CO)_3$ (m = 1)[41] $Fe(CO)_4$ (**4**, m = 2)[42]} or intramolecular base addition[43–45] may stabilise the Sn(II) environment.

^{119}Sn NMR solution spectra are sensitive probes for the chemical environment of tin nuclei in stannylenes. The absorption bands differ strongly in linewidth and chemical shift. For example, the dimeric di(*tert*-butoxy)stannylene **1**, in solution at room temperature, shows a sharp resonance at −93 ppm[41] whereas the monomeric cyclic planar stannylene $\{Sn[(N(^tBu)]_2\text{-}Si(CH_3)_2]\}$ exhibits a very broad resonance at +639 ppm.[46] Heteronuclear temperature-variable NMR spectroscopy has only been scarcely used to investigate dynamic structural changes in alkoxy compounds,[47–50] like for the neopentoxy stannylene $[Sn(\mu\text{-}ONep)_2]_\infty$.[51] Transition metal organometallic complexes of stannylenes, to the best of our knowledge, have not been investigated for their dynamic behaviour so far.

In this paper, we provide a series of new tri- and tetranuclear group 6 carbonyl complexes with **1** as a ligand. We report their syntheses, solid-state molecular structures and spectroscopic characterisation in solution. Temperature-dependent heteronuclear NMR experiments are discussed in detail to propose a mechanism for the observed fluxionality in solution. Over the long run, we want to develop a synthetic protocol for the preparation of mixed group-6–tin compounds with adjustable

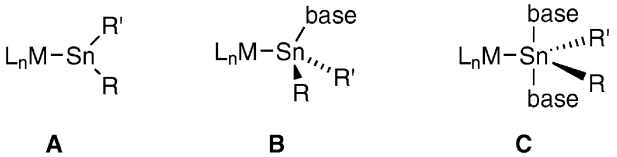

A **B** **C**

Fig. 1 Commonly observed structural types of stannylene transition metal complexes.

† Electronic supplementary information (ESI) available: additional details on X-ray structure and NMR data (correlations). See http://www.rsc.org/suppdata/nj/b4/b414662j/

DOI: 10.1039/b414662j

stoichiometric ratios between their metal components as suitable single-source precursors for the preparation of new materials.

Experimental

General

The reactions were performed under inert nitrogen atmosphere in a Schlenk apparatus. The solvents (THF, hexane, benzene, toluene) were distilled from sodium and kept under nitrogen. $[Sn(\mu\text{-}O^tBu)(O^tBu)]_2$ (**1**) was prepared according to the literature procedure (yield 90%).[2,3] $[M(CO)_6]$ (M = W, Cr) were purchased from Aldrich and used as received.

The photolysis was performed for *ca.* 45 min (IR monitoring) in a Heraeus photoreactor with a 150 W mercury water-cooled lamp and quartz mantle. The solution IR spectra were recorded in KBr cuvettes on a BioRad FTS165. The NMR spectra were recorded on Bruker 200 NMR ACF and ACP spectrometers. High-resolution MS data were measured on a MAT-95 from Finnigan to confirm the elemental composition in the molecular peak. Analytical data were measured on a CHN-900 from LECO. Most samples (**2a**, **2b**, **3b** and **3c**) repeatedly showed a considerably lower content of carbon and hydrogen than calculated. This may be due in part to carbide formation during the combustion and high sensitivity of the compounds. Lineshape analyses of the temperature-variable ^1H NMR spectra were performed using the programmes MacNUTS (Acorn NMR Inc., spectra development) and DNMR.[1]

Syntheses

$\{[(OC)_5M][Sn(\mu\text{-}O^tBu)(O^tBu)]_2\}$ [M = Cr (2a), W (2b)]. In a typical reaction, to a solution of 1.10 g (2.08 mmol for **2a**) or 1.14 g (2.15 mmol for **2b**) $[Sn(\mu\text{-}O^tBu)(O^tBu)]_2$ (**1**) in *ca.* 5 ml of THF is added a freshly prepared solution of $[M(CO)_5(THF)]$ {from $[M(CO)_6]$, M = Cr: 460 mg, 2.09 mmol; M = W: 727 mg, 2.07 mmol} in 190 ml of THF. The reaction is complete within 5 min as seen in the IR spectra. The solvent is then removed under vacuum and the remaining solid [slightly greenish (**2a**) or off-white (**2b**)] re-dissolved in *n*-hexane, concentrated and kept at *ca.* −10 °C. Yellow, transparent crystals form overnight. The isolated yield is 52% (**2a**) and 60% (**2b**). Anal. found (calcd) in % for **2a**: C 29.98 (34.94), H 4.08 (5.03); **2b**: C 26.60 (29.54), H 3.74 (4.25); HR-MS (EI, Δ *m*/*z*) **2a**: 723.9799 (0.8) $C_{21}H_{36}CrO_9Sn_2$, **2b**: 855.9912 (0.0) $C_{21}H_{36}O_9Sn_2W$; IR (*n*-hexane) **2a**: 2062(m), 1955(s), 1950(vs), 1925(m), **2b**: 2070(m), 1945(vs), 1924(vs) cm^{-1}; NMR (δ, *J*/Hz, r.t.]) **2a**: ^1H (benzene; rel. integral) 1.45(1), 1.38(1), 1.36(2); ^{13}C (benzene) 224.1 (C *trans* to Sn, $^2J_{CSn}$ 69.4), 218.0 C (*cis* to Sn, $^2J_{CSn}$ 125.2), 77.9 (μ-*C*Me$_3$, $^2J_{CSn}$ 5.9), 73.6, 72.1 (term. *C*Me$_3$, $^2J_{CSn}$ 6.3; 4.9), 35.7, 34.7 [br, term. C(*C*H$_3$)$_3$, $^3J_{CSn}$ 25; 10], 33.1 [μ-C(*C*H$_3$)$_3$, $^3J_{CSn}$ 22.8]; ^{119}Sn (benzene) 127.7 (*Sn*–Cr), −108.3 ($^2J_{SnSn}$ 203/21, $^{117/119}Sn$); **2b**: ^1H (benzene; rel. integral) 1.48(1), 1.42(2), 1.37(1); ^{13}C (benzene) 199.3 (*CO trans* to Sn, $^1J_{CW}$ 164, $^2J_{CSn}$ 128), 197.6 (*CO cis* to Sn, $^1J_{CW}$ 124, $^2J_{CSn}$ 61/64), 78.1 (br, μ-*C*Me$_3$), 73.8, 72.2 (term. *C*Me$_3$, $^2J_{CSn}$ not observed; 10), 35.7, 34.8 [term. C(*C*H$_3$)$_3$, $^3J_{CSn}$ 24; not observed], 33.4 [μ-C(*C*H$_3$)$_3$, *J* 22, 11]; ^{119}Sn (benzene) −70.5 ($^1J_{WSn}$ 1463), −117.1 ($^2J_{SnSn}$ 182).

$\{[(OC)_5Cr][(OC)_5W][Sn(\mu\text{-}O^tBu)(O^tBu)]_2\}$ (3a). In a typical reaction, a freshly prepared solution of $[Cr(CO)_5(THF)]$ {from $[Cr(CO)_6]$, 280 mg, 1.27 mmol} in 190 ml of THF is added to 1.09 g (1.27 mmol) solid **2b**. The reaction is complete within 5 min as seen in the IR spectra. The volume is reduced under vacuum to *ca.* 3 ml, to which the same amount of toluene is added; removal of the solvent is continued until a solid starts to form at the glass wall. The solution is kept at *ca.* −10 °C. Big yellow, transparent crystals form overnight. The isolated yield is 45% **3a**. Anal. found (calcd) in % for **3a**: C 28.17 (29.17), H 3.38 (3.47); HR-MS (EI, Δ *m*/*z*) 1047.906 (0.1) $C_{26}H_{36}CrO_{14}Sn_2W$; IR (*n*-hexane): 2076(m), 2065(m), 1957(vs), 1952(vs), 1920(m) cm^{-1}; NMR (δ, *J*/Hz, r.t.): ^1H (benzene; rel. integral) 1.45(1), 1.39(1), 1.36(2); ^{13}C (benzene) 223.0 (Cr*C*O *trans* to Sn), 217.4 (Cr*C*O *cis* to Sn, $^2J_{CSn}$ 121), 197.3 (W*C*O *trans* to Sn), 197.0 (W*C*O *cis* to Sn, $^1J_{CW}$ 124, $^2J_{CSn}$ 56), 80.7 (μ-*C*Me$_3$), 74.3, 74.2 (term. *C*Me$_3$, $^2J_{CSn}$ 9; not observed), 34.6, 34.5, {[term. C(*C*H$_3$)$_3$], 32.7 [μ-C(*C*H$_3$)$_3$]}; ^{119}Sn (benzene) 102.6 (*Sn*–Cr), −84.2 (*Sn*–W, $^1J_{WSn}$ 1492, $^2J_{SnSn}$ 158).

$\{[(OC)_5M]_2[Sn(\mu\text{-}O^tBu)(O^tBu)]_2\}$ [M = Cr (3b), W (3c)]. In a typical reaction, a solution of 0.715 g (0.99 mmol **2a**) or 1.62 g (1.91 mmol **2b**) in *ca.* 5 ml of THF are added to a freshly prepared solution of $[M(CO)_5(THF)]$ {from $[Cr(CO)_6]$, 220 mg, 0.99 mmol or $[W(CO)_6]$, 705 mg, 2.00 mmol, respectively} in 190 ml of THF. The reaction is complete within 5 min as deduced from the IR spectra. The volume is reduced under vacuum to *ca.* 3 ml, to which the same amount of toluene is added; removal of the solvent is continued until solid starts to form at the glass wall. The solution is kept at *ca.* −10 °C. White crystals form overnight. The isolated yield is 53% **3b** and 47% **3c**. Anal. found (calcd) in % for **3b**: C 32.80 (34.14), H 3.65 (3.97); **3c**: C 21.73 (26.73), H 2.40 (3.08); HR-MS (EI, Δ *m*/*z*) **3b**: 915.8957 (0.1) $C_{26}H_{36}Cr_2O_{14}Sn_2$, **3c**: 1179.916 (0.5) $C_{26}H_{36}O_{14}Sn_2W_2$; IR (*n*-hexane) **3b**: 2063(m), 1985(w), 1957(vs), 1950(vs), 1922(m), **3c**: 2069(m), 1945(s), 1931(vs), 1893(m) cm^{-1}; NMR (δ, *J*/Hz, r.t.) **3b**: ^1H (benzene; rel. integral) 1.45(1), 1.37(1); ^{13}C (benzene) 223.2 (*CO trans* to Sn), 217.5 C (*CO cis* to Sn), 80.7, 74.3 (*C*Me$_3$), 34.5, 32.7 [C(*C*H$_3$)$_3$]; ^{119}Sn (benzene) 110.8 ($^2J_{SnSn}$ 170); **3c**: ^1H (benzene; rel. integral) 1.46(1), 1.37(1); ^{13}C (benzene) 197.7 (*CO trans* to Sn), 197.1 (*CO cis* to Sn), 80.9, 74.3 (*C*Me$_3$), 34.6, 33.0 [C(*C*H$_3$)$_3$]; ^{119}Sn (benzene) −92.4 ($^1J_{WSn}$ 1485, $^2J_{SnSn}$ 137).

Crystallographic details‡

X-Ray crystallography was performed with a STOE IPDS diffractometer with Kα radiation (λ = 0.710 73 Å). Structures were solved by direct methods and refined by full-matrix least-square methods on F^2 with SHELX-97.[4] Hydrogen atoms were refined as rigid groups with the attached carbon atoms. Drawings were made with CrystalMaker.[5]

2a. $C_{21}H_{36}CrO_9Sn_2$, *M* = 721.88; crystal system: monoclinic, unit cell dimension: *a* 10.238(2), *b* 17.010(3), *c* 17.600(4), β 91.03(3)°, *U* 3064(1) Å^3, $P2_1/n$ (no. 14), *Z* 4, *T* 293(2) K, μ 2.004; 4903 reflections were measured and used in all calculations. The final R_1 was 0.0638 [$wR(F^2)$ was 0.1824 (all data)].

2b. $C_{21}H_{36}O_9Sn_2W$, *M* = 853.73; crystal system: monoclinic, unit cell dimension: *a* 10.212(2), *b* 16.968(3), *c* 17.657(4) Å, β 91.45(3)°, *U* 3059(1) Å^3, $P2_1/n$ (no. 14), *Z* 4, *T* 293(2) K, μ 5.411; 17039 reflections were measured, 4610 unique (R_{int} 0.3516), which were used in all calculations. The final R_1 was 0.0964 [$wR(F^2)$ was 0.2410 (all data)]. The data quality suffered from the instability of the crystal.

3a. $C_{26}H_{36}CrO_{14}Sn_2W$, *M* = 1045.78; crystal system: monoclinic, unit cell dimension: *a* 12.550(3), *b* 11.190(2), *c* 13.390(3) Å, β 94.97(3)°, *U* 1873.3(7) Å^3, $P2_1/m$ (no. 11), *Z* 2, *T* 293(2) K, μ 4.716; 4522 reflections were measured, which were used in all calculations. The final R_1 was 0.0616 [$wR(F^2)$ was 0.1990 (all data)].

‡ CCDC reference numbers 256747–256750. See http://www.rsc.org/suppdata/nj/b4/b414662j/ for crystallographic data in .cif or other electronic format.

3b. $C_{26}H_{36}Cr_2O_{14}Sn_2$, $M = 913.93$; crystal system: monoclinic, unit cell dimension: a 12.559(3), b 11.177(2), c 13.217(3) Å, β 95.24(3)°, U 1853.4(7) Å^3, $P2_1/m$ (no. 11), Z 2, T 293(2) K, μ 1.959; 3460 reflections were measured, which were used in all calculations. The final R_1 was 0.0331 [$wR(F^2)$ was 0.0868 (all data)].

Results and discussion

Syntheses of the compounds

The stannylene complexes **2a**, **2b** and **3a**, **3b** and **3c** are synthesised (Fig. 2) according to the indirect photolysis approach introduced by Strohmeier.[52] The trinuclear stannylene complexes **2a** and **2b** form instantly (IR monitoring) from the THF-stabilised group 6 pentacarbonyl fragment and **1**. The tetranuclear stannylene complexes **3a**, **3b** and **3c** are synthesised stepwise starting from the trinuclear complexes **2a** or **2b**, respectively. The homobis(transition metal) complexes **3b** and **3c** surprisingly are not accessible directly by adding 2 equiv. of the respective pentacarbonyl moiety. Instead, a variety of compounds are formed as is evidenced by IR and multinuclear NMR spectroscopy of the reaction mixtures. It is possible that by disproportionation of the pentacarbonyl moieties $[W(CO)_n]$ ($n = 3$, 4) species are formed that disrupt the integrity of **1**, from which multinuclear complexes with different metal-to-metal ratios might result. Neither was it yet possible to deduce the chemical composition of these compounds nor could any product be isolated.

The trinuclear complexes **2a** and **2b** are isolated by crystallisation from hexane, whereas the tetranuclear complexes **3a**, **3b** and **3c** are crystallised from the reaction solution by reducing the volume after adding toluene. The yields of the off-white powders or slightly yellow crystals are moderate. The solids are very well soluble in THF and well soluble in toluene and hexane (**2a** and **2b**). The compounds are not volatile at reduced pressure (*ca.* 10^{-2} bar) up to 140 °C, which makes their use in CVD processes unsuitable.

Solid-state structure determinations

Crystals suitable for X-ray diffraction could be grown for all complexes. Due to a high anisotropic X-ray absorption, the structure of the tetranuclear complex **3c** could not be solved satisfactorily. However, the heavy atom backbone agrees with that found for the tetranuclear stannylene derivatives **3a** and **3b**. The trinuclear and tetranuclear complexes, respectively, are isotypic and crystallise with 4 and 2 discrete molecules in the unit cell. Ball-and-stick representations of the molecular structures are given in Fig. 3; selected bond lengths and angles are given in Table 1.

The solid-state structures of the complexes can be deduced from the stannylene **1**, whose molecular structure has been determined both in the solid state[3] and in the gas phase.[53] Two stannylene moieties $[Sn(O^tBu)_2]$ form a dimer *via* mutual *tert*-butoxy base addition. The terminal alkoxy groups are found in *anti* positions with respect to the perfectly planar central Sn_2O_2 ring (inversion centre). Differences in molecular parameters in the two physical states are found in the (μ-O)–Sn–(μ-O) angle and in the bond lengths from tin to the bridging and terminal alkoxide O atoms [gas phase/solid state: 76(2)°/73.2(2)°; 2.16(1)/2.128(4) Å; 1.97(2)/2.009(4) Å)]. The bridging oxygen atoms are in a trigonal planar environment with the sum of the bond angles being equal to 358.0°.

Only one solid-state structure of a transition metal complex with **1** as ligand has been reported so far: the diiron complex $\{[(OC)_4Fe]_2[Sn(\mu\text{-}O^tBu)(O^tBu)]_2\}$ (**4**)[42] with two tetracarbonyl transition metal fragments. The trinuclear Mo complex $\{[(OC)_5Mo][Sn(\mu\text{-}O^tBu)(OSiPh_3)]_2\}$ (**5**)[54] with a heteroleptic stannylene ligand is closely related to the pentacarbonyl complexes **2a** and **2b**.

As found from our crystal structure analyses of **2a**, **2b**, **3a** and **3b**, the coordination of transition metal fragments to **1** does not change the main structural features, namely the dimeric structure with a central Sn_2O_2 ring and the *anti* arrangement of the terminal O^{t}Bu groups. This *anti* configura-

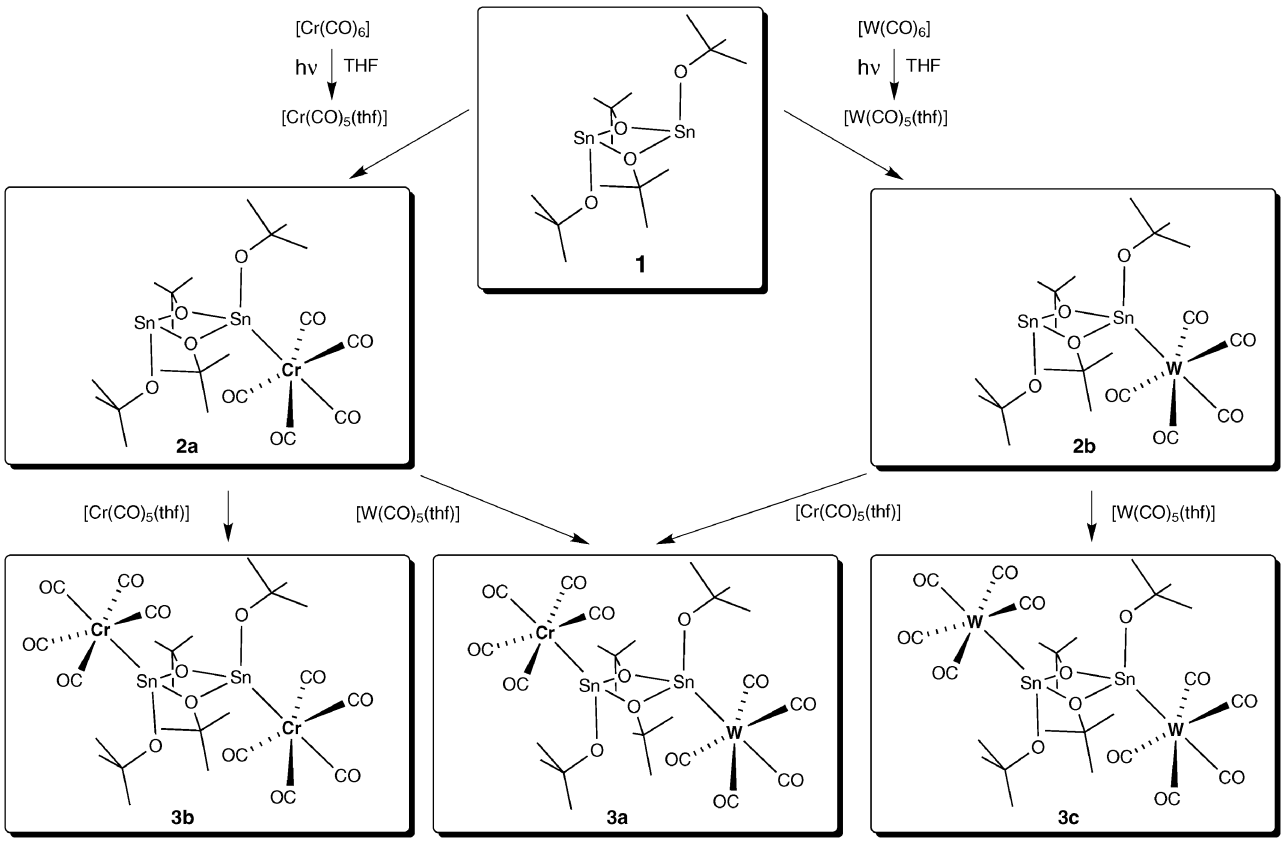

Fig. 2 Synthesis of the alkoxy stannylene complexes **2a**, **2b** and **3a**, **3b**, **3c**.

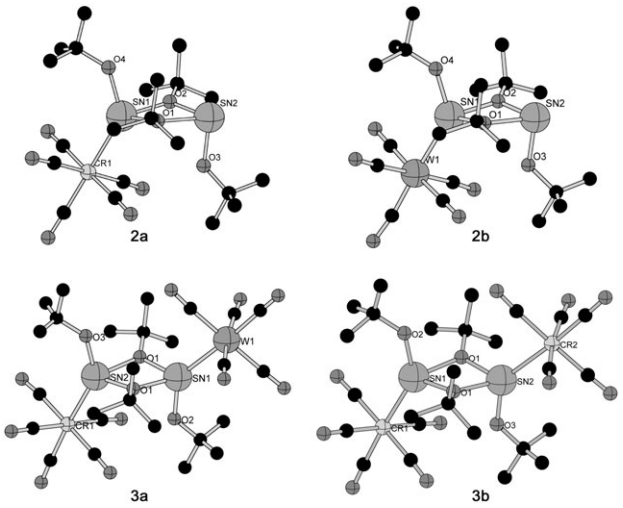

Fig. 3 Plot of the molecular structures of {[(OC)$_5$M][η^1-Sn(O^{t}Bu)(μ-O^{t}Bu)]$_2$} [M = Cr (**2a**), W (**2b**)] and {[(OC)$_5$M][(OC)$_5$M′][μ,$\eta^{1:1}$-Sn(O^{t}Bu)(μ-O^{t}Bu)]$_2$} [M = Cr, M′ = W (**3a**); M = M′ = Cr (**3b**)].

tion is also found in other stannylenes[3,55] and fixed in the calixarene "matrix" [(*para*-^{t}Bu-calix[4]arene)Sn$_2$].[56] However, in analogous germanium compounds[3] the terminal substituents are arranged *syn* to each other with trigonal pyramidal bridging chalcogen atoms, resulting in a strong bending of the M$_2$(μ-E)$_2$ ring. For the complexes discussed herein, the spectral (**2a**, **2b**; **3a**, **3b**, **3c**) and crystallographic (**2a**, **2b**; **3a**, **3b**) data do not give any hint for a second isomer in the *syn* conformation. The oxygen atoms of the bridging O^{t}Bu groups are found in a nearly ideal trigonal planar environment formed by one carbon and two tin atoms. The sums of the bond angles around oxygen vary from 357.4° to 360.0° (both found in **2b**).

Due to the asymmetric coordination in the trinuclear complexes **2a** and **2b**, the tin atoms are found in two different coordination geometries: a Ψ-tetrahedron around Sn1 and a distorted trigonal pyramid around the transition-metal-free Sn2. Both trinuclear compounds **2a** and **2b** have no higher crystallographic point symmetry but are not far from $C_s(m)$. The tetranuclear complexes **3a** and **3b** possess a crystallographic mirror plane, in which tin, transition metal atoms and some atoms of the terminal butoxy groups are placed. The molecular point group in the solid state is therefore C_s.

The distances Sn–Cr in **2a** [2.575(2) Å] and Sn–W in **2b** [2.721(3) Å] are found in the lower half of the range of respective metal–tin(II) bond lengths.[28] A 2004 literature search in the CCDC database shows that the range in bond lengths in group 6 pentacarbonylstannylene complexes varies between 2.527–2.657 Å for neutral chromium–tin (17 complexes with at least one dative Sn→Cr bond) and 2.683–2.821 Å for tungsten–tin [13 complexes; for a discussion of the radius of Sn(II) see ref. 19]. The lowest values are found in polynuclear stannoxane cage molecules,[57,58] whereas the longest bonds are found in monomeric bis-base adducts of stannylene complexes.[59,60] Due to the same covalent radius of Mo and W, the value of the tungsten–tin bond length can be compared to the molybdenum–tin bond length in **5** [2.7449(6) Å]. It seems conceivable that the influence of the terminal group at the attached tin atom (OCR$_3$/OSiR$_3$) on the tin–transition-metal bond is small.

The addition of a second transition metal moiety slightly elongates the tin–transition-metal bonds. The mean Sn–Cr bond length in **3b** [2.61(3) Å] equals that found in **3a** [2.61(2) Å] and is 0.03 Å longer than found in **2a**. The Sn–W bond in **3a** is 0.02 Å longer than the respective bond in **2b**.

Two opposite carbonyl ligands of the pentacarbonyl fragments in the trinuclear complexes adopt a "staggered" configuration with respect to the terminal *tert*-butoxy substituents at both tin atoms (see also the ESI). In the tetranuclear complexes, one of the two pentacarbonyl groups is found in the "staggered", the second [M(CO)$_5$] moiety in the "eclipsed" conformation. It cannot be excluded that crystal packing may have an impact on the sterically unfavourable conformation. It is evident that the steric repulsion in the "eclipsed" conformation causes a slight elongation of the bond length between Cr2 and Sn2 as well as between W1 and Sn1 compared to the "staggered" conformer (see Table 1).

Table 1 Selected bond lengths and angles in the solid state structures of [{(OC)$_5$M}{η^1-Sn(O^{t}Bu)(μ-O^{t}Bu)}$_2$] [M = Cr (**2a**), W (**2b**)] and {[(OC)$_5$M][(OC)$_5$M′][μ,$\eta^{1:1}$-Sn(O^{t}Bu)(μ-O^{t}Bu)]$_2$} [M = Cr, M′ = W (**3a**); M = M′ = Cr (**3b**)][a]

Parameter	**2a**	**2b**	**3a**	**3b**
Sn$_M$–M	2.575(2) st	2.721(1) st	Cr: 2.61(2) st W: 2.740(1) ec	2.60(4) st 2.62(3) ec
Sn$_{noM}$–term-O^{t}Bu	1.962(7)	1.98(1)	—	—
Sn$_M$–term-O^{t}Bu	1.953(7)	1.96(1)	Cr: 1.924(8) W: 1.983(8)	1.964(4) /1.963(4)
Sn$_{noM}$–μ-O^{t}Bu	2.162(6) 2.165(6)	2.13(1) 2.15(1)	—	—
Sn$_M$–μ-O^{t}Bu	2.079(6) 2.071(6)	2.08(1) 2.09(1)	Cr: 2.115(5) W: 2.105(5)	2.106(5) 2.11(1)
trans-M–CO*	1.83(1)	1.90(2)	Cr: 1.87(1) W: 2.01(2)	1.86(3) 1.89(1)
cis-M–CO*	1.87(1)–1.89(1)	1.97(2)–2.02(2)	Cr: 1.92(1)–1.94(1) W: 2.03(2)–2.06(2)	1.89(2)–1.91(2)
Sn–(μ-O^{t}Bu)–Sn	104.8(2) 105.0(3)	104.9(4) 105.8(3)	105.3(2)	105.3(1)
(μ-O^{t}Bu)–Sn$_M$–(μ-O^{t}Bu)	75.8(3)	74.8(4)	Cr: 73.6 W: 74.0(3)	73.79(9)
(μ-O^{t}Bu)–Sn$_{noM}$-(μ-O^{t}Bu)	72.2(2)	72.6(4)	—	—
(term-O^{t}Bu)–(Sn$_M$O$_2$)	102.4(3)	102.8(5)	84.7(1) 86.0(1)	88.0(3) 87.7(3)
(term-O^{t}Bu)–(Sn$_{noM}$O$_2$)	91.1(3)	88.3(5)	—	—
(term-O^{t}Bu)–(Sn$_M$)–M	135.6(3)	134.5(4)	Cr: 142.1(3) W: 137.2(3)	137.6(1) 142.5(1)
(Sn1-μ-O$_2$)–(Sn2-μ-O$_2$)	12.9(2)	12.0(4)	14.6(2)	12.9(1)

[a] Sn$_M$ designates the coordinated tin atom; Sn$_{noM}$ the uncoordinated Sn; *: *trans* and *cis* with respect to Sn; st: staggered, ec: eclipsed, see text).

The number of coordinated transition metal fragments and kind of $[M(CO)_5]$ rotamers also influences the bond angles around tin. Whereas the angle M–Sn_M–(terminal O) is invariant of the kind of transition metal it increases with addition of a second pentacarbonyl fragment (Table 1). This angle is smaller in the diiron compound **4** (135.0°), which can be attributed to the lower steric demands of the tetracarbonyl fragments. The angle between the Sn–transition-metal bond and the Sn_2O_2 plane is considerably widened at the "eclipsed" fragment (see Table 2). The determining factor for the size of this bond angle in the tetranuclear complexes seems therefore to be the transannular repulsion [CO–(term-O^{t}Bu)].

The angle between the Sn–(term-O^{t}Bu) bond and the adjacent SnO_2 plane clearly depends on the substitution pattern. In **1** (96.8°), the Sn–O bonds are bent away from the centre of the molecule. In the trinuclear complexes at the uncoordinated tin atom, it decreases to 91.1(3)°/88.3(4)° (**2a**/**2b**), whereas at the coordinated tin atoms, the O^{t}Bu groups are bent further away [102.4(3)°/102.8(4)°]. In the tetranuclear complexes, steric crowding forces the terminal substituents closer together, the respective angles decrease to 89.7(1)°/88.0(1)° (**3a**) and 88.0(3)°/87.7(3)° (**3b**).

Both (μ-O)–C(CH_3) bonds are tilted against the Sn_2O_2 plane to the same side. In **1** and the tetranuclear complexes **3**, due to the mirror plane, the two angles are equivalent. It is reduced from 20.1° in **1** to 5.9° (**3b**) and 6.3° (**3c**) in the tetranuclear complexes, which most probably comes from steric crowding on both sides of the central Sn_2O_2 plane. In the trinuclear complexes, the residues point away from the side occupied by the pentacarbonyl group. The angles are very different from each other (**2a**: 20.6/39.4°; **2b**: 25.9/4.7°), reflecting a high flexibility of the ^{t}Bu substituents in the search for the least amount of repulsion within the molecule.

The transition-metal–carbonyl C bonds, as expected, show strong a trans influence by the stannylene ligand: the trans metal–O bond is shorter than the cis ones (see Table 1). The overall mean transition-metal–carbonyl C bond length is reduced when one carbonyl is replaced by the stannylene ligand in the group 6 hexacarbonyls {$[W(CO)_6]$: 2.048,[61] 2.026 Å;[62] $[Cr(CO)_6]$: 1.909,[63] 1.915–1.916 Å[64–66]}. This finding parallels that of the respective pentacarbonyl phosphine complexes[67] and is in accord with a balanced σ–π interaction between the transition metal and the carbonyl ligand.[68] However, the umbrella effect, which has been reported for several transition metal complexes with subvalent tin ligands,[59] is not seen with the dimeric stannylene ligands discussed herein. The average values for the angles Sn–M–(*cis*-CO) are close to orthogonality [89.7(6)°–91.5(4)°].

Within the Sn_2O_2 ring, the mean oxygen–tin bond length is slightly reduced on coordination of transition metal fragments [**1**: 2.128 Å, **2a**/**2b**: 2.119(7)/2.11(1) Å, **3b**/**3a**: 2.108(5)/2.110(8) Å]. Addition of one transition metal fragment causes a significant deviation from the regular rhombic geometry found in **1**. The bonds from the coordinated tin Sn_M to the bridging oxygen atoms are shortened while the bonds to the transition-metal-free tin atom are elongated (Table 1), which increases the bond angle (μ-O)–Sn_M–(μ-O) (**1**: 73.2°) and decreases the opposite angle at Sn_{noM}. The *endohedral* bond angle (μ-O)–Sn_M–(μ-O) correlates with the Sn_M–(μ-O) bond length at the coordinated tin atom: the angle decreases with increasing distance. In a plot bond angle *vs.* bond length, two categories may be defined: trinuclear complexes with short bond/obtuse angle and tetranuclear complexes with long bond length/acute angle (see ESI). Due to the steric demand of the pentacarbonyl group, it becomes obvious that the shortening of the adjacent tin–oxygen bond must be due to electronic rather than steric effects. In a simple picture, the electron demand of the coordinating metal must have an influence on the adjacent bonds at tin. The same trend is observed on coordination of planar ring systems like cyclo-P_3 ligands.[69]

The tin–oxygen bond lengths to the terminal butoxy groups are significantly reduced upon addition of pentacarbonyl groups, without correlation with the number or kind of transition metal [**1**: 2.009(4) Å]; in the trinuclear complexes those at the coordinated tin atom (Sn_M) are more reduced than the those at the transition-metal-free one (Table 1).

On coordination, the central Sn_2O_2 ring deviates from planarity. The dihedral angle between the SnO_2 planes along the μ-O···μ-O vector is independent of the substitution pattern (**2a**: 12.9°; **2b**: 12.0°; **3a**: 14.6°; **3b**: 12.9°) but stronger than the respective angles in **5** (7.2°) and **4** (0.0°, crystallographic inversion centre). One consequence of the bending of the Sn_2O_2 ring is the reduced distance between the tin atoms. While in the stannylene **1**, 3.44 Å is found,[3,53] all transition metal complexes have Sn···Sn distances of 3.35 Å.

An interesting structural analogue to the tetranuclear complexes is found in the bis-inidene complexes $\{[(OC)_5M]_2[Sn(\mu\text{-}OEt)]\}_2^{2-}$ (M = Cr, W) characterised by Huttner *et al.*[70] Two 7-electron terminal OR^- residues in **3** are formally substituted by the isolobal 17-electron $[M(CO)_5]^-$. With respect to **3b**, the bond angles in the planar four-membered ring at tin become more acute with a higher number of pentacarbonyl fragments [70.8(4)–72.8(1)°] and the Sn–Cr bond lengths are elongated [2.635(3)–2.654(2) Å], which might be due to steric repulsion and the higher electron density at Sn. The Cr–Sn–Cr angles are more acute [124.4(8)–125.22(8)°], in accord with the transannular repulsion argument (*vide supra*).

The observed changes in bond lengths and angles clearly show that, when transition metal fragments are added to $[Sn(O^tBu)_2]_2$ (**1**), the hybridisation of the orbitals around tin is affected. In a simple picture, the lone pair s-orbital on complexation becomes involved in bonding and therefore the p^3-bonding state of tin becomes more sp^3. At the same time, electron withdrawal by the metal fragments induces shorter Sn–O bonds.

Spectroscopic features

IR spectroscopy. The complexes **2a**, **2b** and **3a**, **3b**, **3c** in the carbonyl stretching region show the typical pattern for pentacarbonyl fragments with approximate C_{4v} symmetry around the central metal. The homobis(transition metal) complexes **3b** and **3c** in solution each show only one pattern, without a hint of cooperative effects between the two $[M(CO)_5]$ groups. The mixed tetranuclear complex **3a** shows two sets of bands for the chromium and tungsten pentacarbonyl groups. The wavenumbers of the tetranuclear complexes correspond to the values in the respective trinuclear complexes. The values and relative intensities compare very well to phosphine complexes and other pentacarbonyl stannylene complexes irrespective of the

Table 2 M–Sn_M–(term-O^{t}Bu) angle and M–Sn_M–Sn_2O_2 plane in the trinuclear (**2a**, **2b**) and tetranuclear stannylene complexes (**3a**, **3b**); Sn_M designates the transition metal coordinated tin atom (st: staggered. ec: eclipsed)

Parameter/°	**2a**	**2b**	**3a**	**3b**
M–Sn_M–(term-O^{t}Bu)	Cr_{st}: 135.6(3)	W_{st}: 134.5(4)	Cr_{st}: 142.3(3) W_{ec}: 137.2(3)	Cr_{st}: 142.5(1) Cr_{ec}: 137.6(1)
M–Sn_M–(Sn_2O_2)	Cr_{st}: 121.7(2)	W_{st}: 122.2(3)	Cr_{st}: 121.8(2) W_{ec}: 142.7(1)	Cr_{st}: 122.0(1) Cr_{ec}: 142.5(1)

substituents on tin,[36,40,41,71] giving evidence for similar electronic (donor/acceptor) properties (see structure discussion above).

Room temperature $^{119}Sn\{^1H\}$ NMR spectroscopy. In all ^{119}Sn NMR spectra, singlets appear with satellites due to coupling with $^{117/119}Sn$ (**2a**, **2b**, **3a**) or ^{117}Sn (**3b**, **3c**). The tungsten derivatives are characterised by ^{183}W satellites (low-field signal in **2b**, Fig. 4; high-field signal in **3a**).

Base coordination on stannylenes causes an upfield drift of the ^{119}Sn resonances,[72,73] whereas a deshielding for Lewis acids adducts like BF_3 is observed.[12] With transition-metal-complex fragments,[26,72,73] the coordination deshielding ($\Delta\delta_{coord} = \delta_{free\ molecule} - \delta_{ligand}$) on the respective tin atom decreases going down the periodic table: in the series of the tri-/tetranuclear complexes it falls with the same magnitude from chromium ($\Delta\delta_{coord}$: **2a** 220 ppm; **3b** 201 ppm) to tungsten ($\Delta\delta_{coord}$: **2b** 21 ppm; **3c** 1 ppm). For the trinuclear complexes $\{[(OC)_5Mo][Sn(\mu\text{-}O^tBu)(OSiPh_3)]_2\}$ (**5**)[54] and $\{[(OC)_3Ni][Sn(O^tBu)_2]_2\}$ (**6**)[41] $\Delta\delta_{coord} = 202$ ppm and 244–255 ppm are calculated. The complexation of one tin atom in the trinuclear complexes as **2a** and **2b** also influences the second tin nucleus in the bis-stannylene, an effect that is known also from other coupling (element)$_2$ units.[74] However, the resonance for the free tin atom is less influenced [$\delta(^{119}Sn)_{free\ tin}$: −108 (**2a**), −117 (**2b**) ppm]. The overall influence of the coordination on the magnetic resonance of the "Sn_2 pair" is seen in the total coordination chemical shift difference $\Delta\bar{\delta}$, which compares the average ^{119}Sn chemical shift of the coordinated ligand with that of the free molecule $[Sn_2(O^tBu)_4]$ (**1**). $\Delta\bar{\delta}$ increases with increasing difference in (number of coordinated chromium fragments) minus (number of coordinated tungsten fragments) in the order **2b** ≈ **3c** < **3a** < **2a** < **3b** [$\Delta\bar{\delta}$ (ppm) = −1; 1; 83; 101; 202]. The heteroleptic molybdenum complex **5** shows an intermediate value of 82.5 ppm,[54] the mononickel complex **6** around 250 ppm,[41] the bis-adducts $\{[(OC)_3Ni]_2[Sn(OSiMe_3)(\mu\text{-}OSiMe_3)]_2\}$ at 294.2 ppm[41] and the bis-iron complex $\{[(OC)_4Fe]_2[Sn(O^tBu)(\mu\text{-}O^tBu)]_2\}$ 128.4 ppm,[42] which is surprisingly low in this context.

The tin-tungsten coupling constant increases with the number of added transition metal fragments. The observed coupling constants are in the range of previously reported direct ^{183}W-^{119}Sn coupling constants.[26,73,75,76] Considerably smaller values are found for five-coordinate tin, chelating substituents (894–976 Hz)[60,77] and half-sandwich complexes (610 Hz).[78]

The integrity of the Sn_2O_2 central cycle is clearly evidenced by the presence of ^{119}Sn-$^{119/117}Sn$ coupling. For **3b**, the ratio of the individual coupling constants $^2J(^{119}Sn$-$^{117/119}Sn)$ of 1.050 agrees well with the theoretically expected value for the ratio of the gyromagnetic constants (1.046). ^2J increases in the order **3c**, **3a**, **3b**, **2b**, **2a** (137, 158, 170, 182, 208 Hz), which are above the values for stannylenes $\{[RR'Sn_2(\mu\text{-}O^tBu)_2]$, R = $OSiMe_3$, R′ = $N(SiMe_3)_2$, $OSiMe_3$ and R = R′ = O^tBu (**1**): 72, 60 and 88 Hz[79]$\}$ and **5** (92 Hz).[54] There is a clear linear correlation of J with the chemical shift ∂ of the coordinated tin atom according to the nature of the transition metal (see Fig. 5) with similar slope for both series [2.02 Hz ppm^{-1} (Cr), 1.93 Hz ppm^{-1} (W)]. The difference in coordination deshielding power of Cr and W can be calculated from the difference at $\Delta\delta$ ($J = 0$) = 186 ppm, which is similar to the 200 ppm calculated from individual shifts (*vide supra*). The trinuclear complexes are found to the left (see Fig. 5), the deshielding is more efficient than in the bis(transition metal) complexes. This dependence indicates that the coordination of the transition metal has an impact on the electronic communication between the tin atoms, which parallels our findings from the structural analysis (*vide supra*).

Examination of the structural and spectroscopic data reveals that $^2J_{Sn\text{-}Sn}$ (measure of the s character of the MOs) increases with increasing bond angle (measure for hybridisation around tin; see ESI). Relationships between the electronegativity of the substituents, coordination deshielding, chemical shift and coupling constant with structural parameters have been discussed only occasionally.[72,80]

Room temperature ^1H NMR spectroscopy. The ^1H NMR spectra at room temperature in benzene solution show three signals in the integral ratio 1 : 1 : 2 for **2a** and two signals in the integral ratio 1 : 3 for **2b**. The linewidth of the signals differs strongly. This points to an (intramolecular) dynamic rearrangement of the alkoxy substituents. The spectra of the homo-bis(transition metal) complexes show two singlets of equal intensity, and for the heterobis(transition metal) **3a** a 1 : 1 : 2 integral ratio is found. The integral ratio in the heterobis (transition metal) complex makes it probable that the low-field signal in the homobis(transition metal) complexes **3b** and **3c** is attributable to the bridging butoxy groups, but the temperature-dependent shift makes it more probable that the high-field signals have to be attributed to the bridging O^tBu groups (*vide infra*).

Room temperature $^{13}C\{^1H\}$ NMR spectroscopy. In the CO region, two signals for four cis and one trans CO ligands point to an idealised C_{4v} local point of the pentacarbonyl fragment, which indicates that the rotation around the transition-metal–tin bond is unhindered at room temperature (see also IR spectroscopy). The degree of π-backbonding from the transition

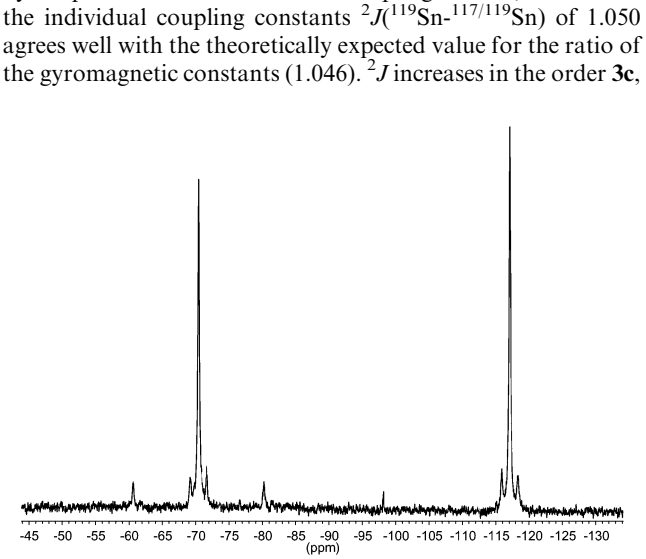

Fig. 4 ^{119}Sn NMR spectrum of **2b** at room temperature. Satellites are due to $^{117/119}Sn$ (smaller constant) and ^{183}W (low-field signal).

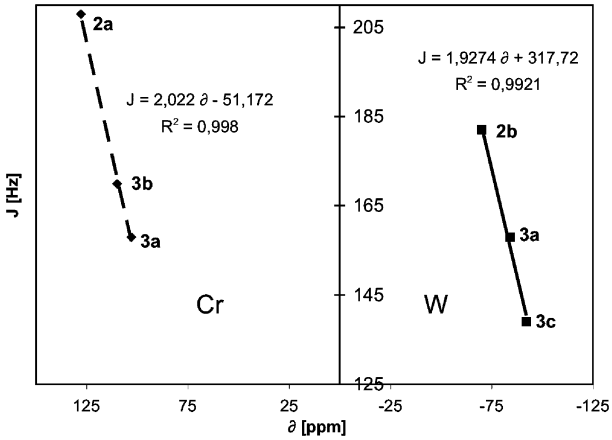

Fig. 5 Correlation of the vicinal $^2J_{Sn\text{-}Sn}$ coupling constant with the ^{119}Sn chemical shift of the coordinated tin atom in the complexes $\{[(OC)_5M]_n[(OC)_5M']_m[Sn(O^tBu)_2]_2\}$ [n = 1, m = 0, M = Cr (**2a**), W (**2b**); $n = m = 1$, M = M′ = Cr (**3b**), W (**3c**), M = Cr, M′ = W (**3a**)] according to the coordinating transition metal (chromium left, tungsten right).

metal is documented in the bond length between the respective carbon atom (cis/trans CO) and the transition metal. This crystallographic number correlates well with the spectroscopic ^{13}C chemical shifts for the complexes **2a**, **2b** and **3a–3c**: the shorter the bond, the higher the absorption frequency (see ESI), which is in agreement with the expected ^{13}C deshielding with increasing π-backbonding.[72] Most carbonyl resonances show satellites due to coupling to ^{183}W and $^{117/119}Sn$. The ratio for the ^{119}Sn- to-^{117}Sn coupling constant in the spectrum for **2b** (cis CO: 1.049) corresponds well with the theoretical value (*vide supra*).

The assignment of terminal and bridging O^{t}Bu substituents in the ^{13}C spectra is not unambiguous since the chemical shift differences are small and integral ratios can only be taken with caution. However, based on significantly higher integral areas in the trinuclear and the heterobis(transition metal) complexes, the most *deshielded* signal in the quaternary carbon region and the most *shielded* signal in the methyl region are attributed to the bridging alkoxy groups. For the heteroleptic ligand in **5**,[54] the bridging O^{t}Bu groups give rise to singlets at 78.7 and 33.3 ppm ($CDCl_3$), which is slightly above/below the respective values for the free stannylene **1** (75.5/33.6 ppm, toluene).[81] For the homobis(transition metal) complexes **3b** and **3c**, the signals are therefore assigned in analogy. The singlets for the *tert*-butyl groups show satellites. Since these are present irrespective of the transition metal, they are ascribed to coupling tin nuclei.

Variable temperature heteronuclear NMR spectroscopy of the distannylene complexes [{(OC)$_5$M}$_n${Sn(O^{t}Bu)(μ-O^{t}Bu)}$_2$] [*n* = 1, M = W (2b), Cr (*n* = 1 (2a), 2 (3b)]. Because the trinuclear complexes at room temperature in the ^1H and ^{13}C NMR spectra show considerable line broadening and integral ratios, which are not in accord with the X-ray molecular structure, temperature-variable NMR investigations have been performed.

Dynamic processes in stannylene molecules are well-known for dimeric alkoxy stannylenes {*e.g.*, [Sn(OR)$_2$]$_2$ with R = Me, Et,[82] ^{t}Bu,[2] Nep[51]}. However, investigations on dynamic processes with stannylenes[83,84] or germylenes[85–87] as ligands in transition metal complexes are limited to rotations around the transition-metal–main-group-element bond. Therefore, a detailed heteronuclear (^1H, ^{13}C, ^{119}Sn) temperature-variable NMR study has been performed on the complexes **2a**, **2b** and **3b**. The exchange mechanism in **1**, which up to now was not been examined in detail,[2] will be discussed elsewhere.[81]

Heteronuclear temperature-variable solution NMR spectra have been obtained for {[(OC)$_5$W][Sn(O^{t}Bu)$_2$]$_2$} [**2b**; 203–408 K (^1H, ^{13}C), 295–403 K (^{119}Sn)] and {[(OC)$_5$Cr]$_n$[Sn(O^{t}Bu)$_2$]$_2$} [*n* = 1 (**2a**), 2 (**3b**); 203–408 K (^1H, ^{13}C)] in toluene (203 to 353 K) and xylene (r.t. to 403 K).

There are three well-separated regimes in the temperature-variable ^1H NMR spectra (in the following the spectra for **2b** are discussed in detail, see Fig. 6 and Table 3; those of **2a** differ only in the absolute values). In the low-temperature range up to 263 K, no dynamic exchange is observed (invariable linewidth); the signal pattern corresponds to the X-ray molecular structure. The signals, which at 303 K (310 K for **2a**) coalesce (integral ratio 1 : 2, thus one terminal and the bridging O^{t}Bu), move towards each other, the third signal (terminal O^{t}Bu) moves in the same direction as the signal for the first terminal O^{t}Bu group. Between 263 and 353 K, the two signals at low- and high-field (integral ratio 1 : 2) coalesce to form one singlet (relative integral 3). Above 373 K, this signal gets significantly broader, as does the signal with intensity 1 (second terminal O^{t}Bu group) above 333 K. This could lead to a second coalescence phenomenon at higher temperature. The ^{13}C NMR spectra are analogous to the ^1H NMR spectra. This behaviour can be explained by an exchange mechanism of all *four* O^{t}Bu groups at high temperature, while at intermediate temperature, only *three* substituents are exchanging on the NMR time scale.

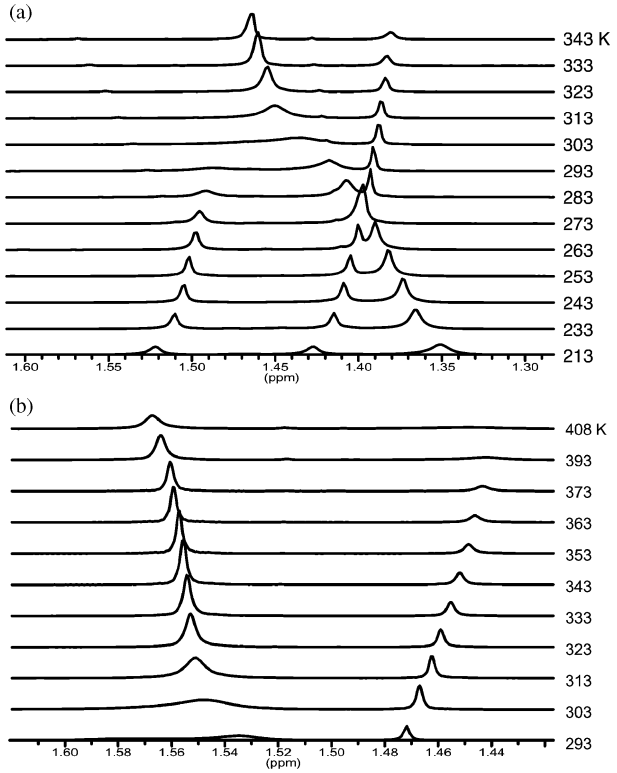

Fig. 6 Temperature variable ^1H NMR spectra of **2b** in the range of (a) 213–343 K (d_8-toluene); (b) 293–408 K (d_{10}-xylene).

The tetranuclear complex **3b**, on the other hand, over the whole temperature range shows two singlets (integral ratio 1 : 1 in ^1H NMR) for the two types of alkoxy groups found in the solid-state molecular structure. The stannylene complex is static in solution.

While in the ^{13}C NMR of **2a**, **2b** and **3b** for the ^{t}Bu resonances there is a negligible drift of the chemical shifts, in the ^1H NMR spectra all the signals show a pronounced drift of the chemical shift with temperature. Interestingly, this drift behaviour is very different for the different signals: while the two low-field resonances (integral ratio 1 : 1, hence terminal O^{t}Bu) in the spectra of **2a** and **2b** move to high field with increasing temperature with a parabolic curvature, the high field signal (rel. integral 2, μ-O^{t}Bu) moves strictly linearly to low field (see ESI). While the chemical shift of the signals for the bridging O^{t}Bu substituents in both complexes are very similar (according to absolute values and slope), the low-field signal is more deshielded in the tungsten than in the chromium derivative, while with the intermediate signal, the situation is reversed. The former signal is ascribed to the O^{t}Bu substituent at the transition-metal-coordinated tin atom, which would be in agreement with the expected deshielding on coordination.

For the tetranuclear **3b**, the high-field signal is basically unchanged over the temperature range studied (213 K: 1.42 ppm; 353 K: 1.44 ppm), while the low-field signal shows a linear increase of the chemical shift value with temperature (see ESI). The slope is similar to that of the singlet with integral ratio 2 in the trinuclear complexes [7.0×10^{-4} ppm K^{-1} (**3b**) *vs.* 6.9×10^{-4} (**2a**) and 7.5×10^{-4} ppm K^{-1} (**2b**)]. This makes the attribution to the bridging O^{t}Bu substituents very probable, although the relative δ values of the bridging and terminal O^{t}Bu groups would then be reversed with respect to the trinuclear and heterobis(transition metal) complexes (*vide supra*).

The most marked drift in the $^{13}C\{^1H\}$ NMR spectra of **2b** is observed for the *trans*-CO resonance (trans with respect to tin): it is shielded linearly with increasing temperature [213 K: 200.1

Table 3 ^{119}Sn NMR data of **2b** at various temperatures (xylene)

	Coordinated Sn				Transition-metal-free Sn		
T/K	δ	$^{1}J_{\text{W-Sn}}$/Hz	$^{2}J_{\text{Sn-Sn}}$/Hz	Linewidth/Hz	δ	$^{2}J_{\text{SnSn}}$/Hz	Linewidth/Hz
295	−64.7	1460	177	20	−111.0	182	20
353	−74.8	1503	184	28	−116.7	Broad	89
403	−84.7	1483	196	25	−122.0	196	21

ppm (toluene), 403 K: 197.8 ppm (xylene); see ESI]. A stronger shielding of the carbon nucleus may be induced by either higher electron density in bonding molecular orbitals (σ-donation from Sn) or depopulation of anti-bonding states (π-accepting Sn).

In the ^{119}Sn{^{1}H} NMR spectra of **2b** several effects are evident with increasing temperature (Fig. 7): Both signals move to higher field, the linewidth of the free (uncoordinated) tin atom goes through a maximum, the tin-tin coupling constant increases and the tin-tungsten coupling constant slightly varies with temperature (± 3%), being highest with the largest linewidth of the signal for the free tin atom.

The fit of the δ values gives a linear slope of 0.19 ppm K^{-1} for the coordinated and 0.10 ppm K^{-1} for the transition-metal-free tin atom to higher field, which is similar to **1** (slope 0.17 ppm K^{-1}).[81] A stronger but inverse temperature drift between 0.2 and 2.0 ppm K^{-1} was observed for base-stabilised and dimeric inidene-type stannylene complexes.[59,70] The drift in the latter was interpreted in terms of an equilibrium between fourfold (predominant at low temperature) and threefold (high temperature) coordination around the tin atom.

A remarkable difference in the two ^{119}Sn NMR signals is the dependency of the linewidth on temperature of only the signal for the transition-metal-free (three-coordinate) tin atom. Since the signal for the corresponding metal-coordinated tin atom is basically unchanged, this phenomenon is not due solely to dynamic exchange. The effect is not yet understood and will be studied elsewhere.[81]

The Sn-Sn coupling constant shows a steady increase with temperature. This might be accounted for by the higher electron density in s-AO-containing MOs, and thus stronger bonding between the two tin atoms at higher temperature. The dissociation of the stannylene ligand into monomeric species is highly improbable on that basis. Support is given by the observations that **2b** in toluene or THF does not dismutate and that free **1** and **3c** do not commutate in toluene at 90 °C after 2 days [eqn. (1)]:

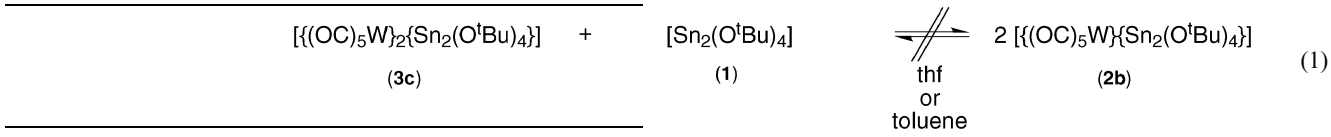

(1)

However, partial formation of the heterobis(transition metal) **3a** is observed when the homonuclear starting materials are mixed and heated for 1 week in toluene solution [eqn. (2)]:

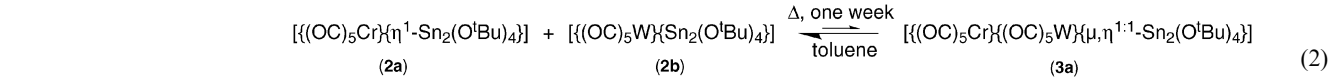

(2)

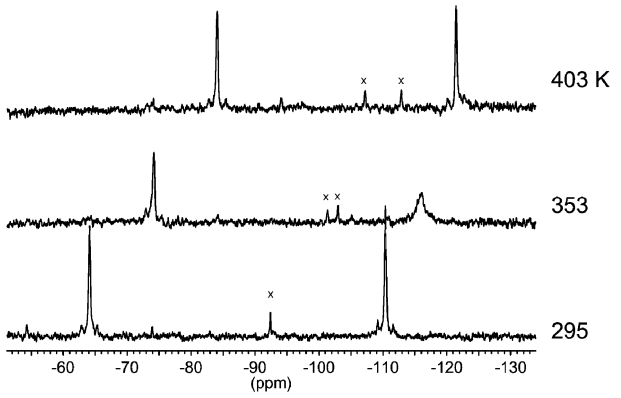

Fig. 7 ^{119}Sn{^{1}H} NMR spectra of **2b** at various temperatures in d_{10}-xylene (x indicates impurities).

These findings differ from those reported by Sita *et al.*,[79] who found that mixing the homoleptic stannylenes [Sn$_2$(O^{t}Bu)$_4$] (**1**) and [Sn$_2$(OSiMe$_3$)$_4$], for example, at room temperature in hexane yields, in a clean and fast reaction, the respective heteroleptic dimeric stannylene [Sn$_2$(OSiMe$_3$)$_2$(μ-O^{t}Bu)$_2$].

The ^{1}H NMR spectra of **2b** (213–293 K in toluene, 293–408 K in xylene) and **2a** (203–353 K in toluene) have been submitted to lineshape analysis[1] to obtain information on the chemical shifts around the coalescence point(s) and especially to calculate the exchange rates for the O^{t}Bu groups. The latter are used to determine the thermodynamic parameters of the exchange mechanisms at low and high temperature, respectively.

Because two coalescence phenomena are clearly separated, two separate exchange mechanisms are simulated and the resulting absorption bands are fitted to the experimental signals by varying δ and exchange rate k. The low-temperature process has been simulated by a 4-nuclear spin, in which one spin is not exchanging with the other 3 mutually exchanging spins. According to the relative ppm values at low temperature, the spins are named *a*, *b*, *c* and *d*, with $c = d$ (equivalent bridging O^{t}Bu), *a* being the exchanging terminal O^{t}Bu and *b* the O^{t}Bu that is not involved in the exchange at low temperature. The exchange rates k_{ba} (spins *b* and *a*), k_{bc} and k_{bd} therefore are equal to zero. The exchange rates k_{ac}, k_{ad} and k_{cd} at a given temperature are equivalent but are non-zero. The inherent linewidth of each signal is constant and deduced from the linewidth at low temperature. At high temperature, the exchange rates with participation of spin *b* (k_{ba}, k_{bc}, k_{bd}) are equivalent but non-zero. Due to limitations in the programme, a satisfactory fit could only be obtained with the signal having relative intensity 1.

The function $\log(k/T)$ of the respective exchange rates k^{LT} (low-temperature process) and k^{HT} (high-temperature process) are plotted against the reciprocal temperature (Eyring plot) to obtain the activation enthalpy $\Delta H^{\neq}$, activation entropy $\Delta S^{\neq}$ and eventually the activation free energy of the process at room temperature $\Delta G^{\neq}_{298} = \Delta H^{\neq} - T\Delta S^{\neq}$ (Fig. 8). Thus, for the low-temperature exchange mechanism occurring for **2b**, values of $\Delta H^{\neq \text{LT}} = 95(3)$ kJ mol^{-1} and $\Delta S^{\neq \text{LT}} = +95(10)$ J mol^{-1}

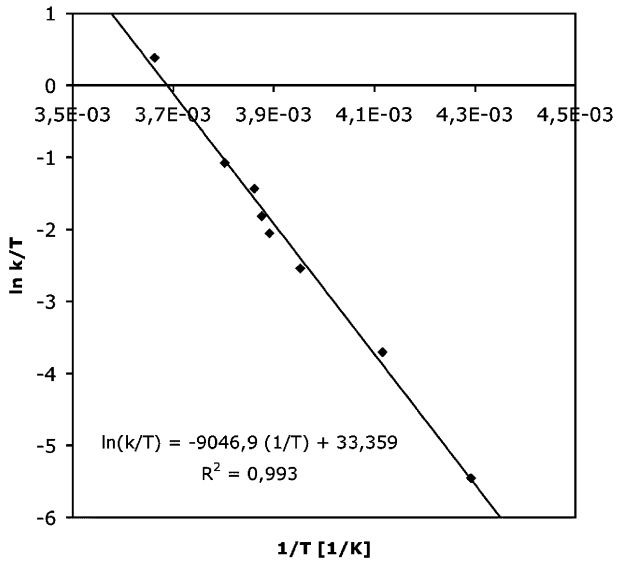

Fig. 8 Eyring plot for the ^{1}H NMR values for the low-temperature exchange mechanism in **2b**.

K^{-1} are calculated. For **2a**, the respective values are similar: $\Delta H^{\neq LT} = 91(3)$ kJ mol^{-1} and $\Delta S^{\neq LT} = +70(10)$ J mol^{-1} K^{-1}. For the high-temperature process in **2b**, values of $\Delta H^{\neq HT} = 82(5)$ kJ mol^{-1} and $\Delta S^{\neq HT} = -30(8)$ J mol^{-1} K^{-1} are calculated. From the Gibbs–Helmholtz equation, $\Delta G^{\neq}{}_{298}{}^{LT} = 70(6)$ (**2a**), 67(6) (**2b**) kJ mol^{-1} and $\Delta G^{\neq}{}_{298}{}^{HT} = 91(7)$ kJ mol^{-1} (**2b**) are obtained.

Proposal for the alkoxide exchange in trinuclear complexes with [Sn(O^{t}Bu)$_2$]$_2$ (1) as ligand

The spectroscopic and structural data presented above contribute to an understanding of the exchange mechanism in the trinuclear complexes. The transition metal fragment does not take an active role in that process, which is seen from the very similar thermodynamic data for compounds **2a** and **2b** and similar spectra. The preservation of the transition-metal–tin bond over the whole temperature range is unambiguously proven by the presence of tungsten satellites at the ^{119}Sn resonance for the coordinated tin atom and $^{117/119}$Sn in the CO region of the ^{13}C NMR. The complexes do not dissociate in solution, at least not to a detectable amount. This is seen from the presence of Sn-Sn coupling over the whole temperature range and is also supported by the cross experiments [eqn. (1) and eqn. (2)]. The bonding situation in the transition state at the transition-metal-free tin atom very likely resembles that of the transition state in the free stannylene ligand (**1**), because of similar drift of the chemical shift and line broadening.[81] However, under these assumptions, there do remain at least four possible pathways for the exchange mechanism at low temperature (Fig. 9).

In the associative pathway *via* **A**, the terminal alkoxy substituent at the coordinated tin atom moves towards the uncoordinated tin atom, thus forming a fourfold coordination at both tin atoms. The inverse way, that is attack of the terminal O^{t}Bu residue on the uncoordinated tin atom onto the coordinated tin atom (**A′**) leads to a transition state in which the tin atoms have coordination numbers 3 and 5. However, because of steric crowding and coordinative saturation, the latter is less probable. The character of the exchanging O^{t}Bu groups in **A** and **A′** would resemble the bridging substituents in the ground state. In the dissociative pathways, one bridging alkoxy substituent moves in a terminal position at the transition-metal-free (**D**) or the coordinated (**D′**) tin atom. In the transition state, three-coordinate (**D**) or four and two coordinate (**D′**) tin atoms would result. The character of the exchanging O^{t}Bu groups would be more like the terminal substituents in the ground state. Again, the pathway *via* **D′** is less likely.

The dissociative pathways are supported by the positive activation entropy and the observation that on heating, the bridging alkoxy substituents become more deshielded than the terminal ones; the proportion of terminal substituents in the equilibrium is increased.

However, there are also quite a number of observations supporting the associative pathways. The coupling constant $^{2}J_{SnSn}$ between the two tin atoms increases with temperature, as does the shielding of the CO resonances, which is conceivable with a stronger interaction. The ^{119}Sn resonances of the metal-free tin atom especially is moving towards low field, which indicates a certain amount of a higher coordination number in the transition state. According to the assignment made above in the ^{1}H NMR spectra, it is very likely that it is the terminal O^{t}Bu substituent at the coordinated tin atom that exchanges with the bridging positions. There is a potentially free coordination site at the transition-metal-free tin atom. The Lewis acidity of three-coordinate tin in dimeric structures has been observed, for example in **5**,[54] where a phenyl ring of a neighbouring $OSiPh_3$ substituent is bond face-on the free stannylene coordination site. Three bridging alkoxy ligands are found in heteromultinuclear alkoxy compounds with tin(II).[88,89]

Based on these arguments, the associative pathway going through **A** seems the most probable one for the low-temperature exchange mechanism. However, we hope to gain more

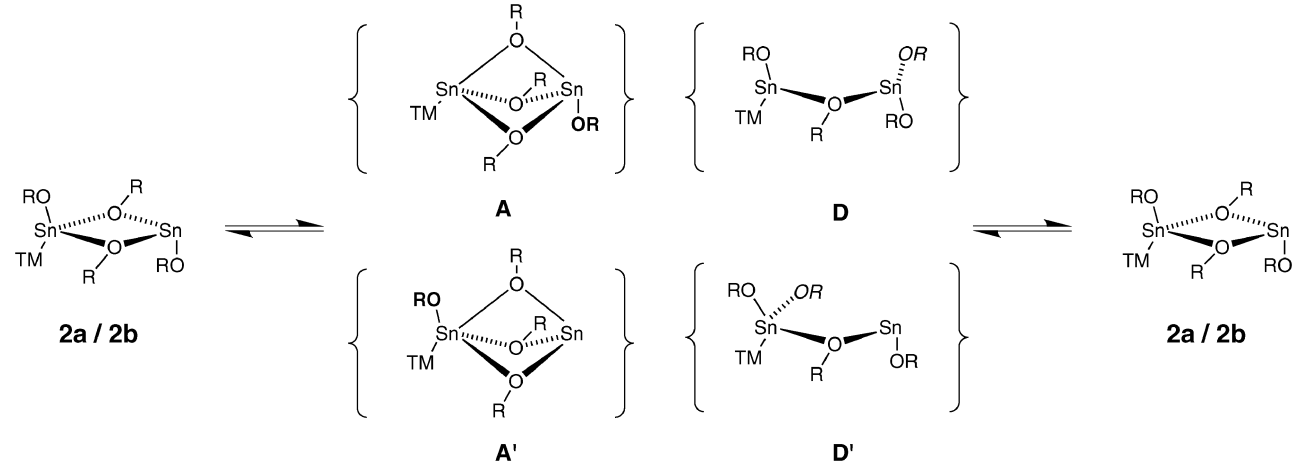

Fig. 9 Possible associative (**A**, **A′**) and dissociative (**D**, **D′**) intermediates of the low-temperature O^{t}Bu exchange mechanism in **2a** and **2b** (TM = transition metal fragment; **bold** in **A**, **A′** designates the static terminal OR, *italic* in **D**, **D′** designates the moving μ-OR).

insight by combined spectroscopic and computational investigations of the parent free ligand **1**.[81]

For the high temperature mechanism, less information is available. Dissociation of the dimeric stannylene is improbable (NMR, cross experiments), but the presence of four bridging O^{t}Bu groups seems very unfavourable. However, it is likely that the exchange of the last alkoxy group is occurring out of the transition state of the low-temperature process: one of the three bridging O^{t}Bu's is exchanging with a terminal substituent at the metal-free Sn.

References

1 H. J. Reich, *Dynamic Nuclear Magnetic Resonance Spectroscopy with DNMR-Pro*, University of Wisconsin, Madison, WI (http://www.chem.wisc.edu/areas/reich/plt/windnmr.htm).
2 M. Veith and F. Töllner, *J. Organomet. Chem.*, 1983, **246**, 219.
3 M. Veith, P. Hobein and R. Roesler, *Z. Naturforsch., B: Chem. Sci.*, 1989, **44**, 1067.
4 G. M. Sheldrick, *SHELX-97, Program for refinement of crystal structures*, University of Göttingen, Germany, 1997.
5 *CrystalMaker*, CrystalMaker Software, Ltd., Yarnton, UK (http://www.crystalmaker.com/).
6 A. Marquez and J. F. Sanz, *J. Am. Chem. Soc.*, 1992, **114**, 2903.
7 M. Veith, *Comm. Inorg. Chem.*, 1985, **4**, 179.
8 M. Veith, *J. Organomet. Chem. Libr.*, 1981, **12**, 319.
9 M. Veith, *Nachr. Chem., Tech. Lab.*, 1982, **30**, 940.
10 M. Veith, *Adv. Organomet. Chem.*, 1990, **31**, 269.
11 (*a*) M. Veith, *Angew. Chem.*, 1987, **99**, 1; (*b*) M. Veith, *Angew. Chem., Int. Ed. Engl.*, 1987, **26**, 1.
12 C. C. Hsu and R. A. Geanangel, *Inorg. Chem.*, 1980, **19**, 110.
13 M. Veith, V. Huch, J. P. Majoral, G. Bertrand and G. Manuel, *Tetrahedron Lett.*, 1983, **24**, 4219.
14 M. Veith and A. Müller, *J. Organomet. Chem.*, 1988, **342**, 295.
15 M. Veith, M. Olbrich, S. Wang and V. Huch, *J. Chem. Soc., Dalton Trans.*, 1996, 161.
16 (*a*) A. Krebs, A. Jacobsen-Bauer, E. Haupt, M. Veith and V. Huch, *Angew. Chem.*, 1989, **101**, 640; (*b*) A. Krebs, A. Jacobsen-Bauer, E. Haupt, M. Veith and V. Huch, *Angew. Chem., Int. Ed. Engl.*, 1989, **28**, 603.
17 M. Veith and O. Recktenwald, *Z. Anorg. Allg. Chem.*, 1979, **459**, 208.
18 M. Veith, M. Nötzel, L. Stahl and V. Huch, *Z. Anorg. Allg. Chem.*, 1994, **620**, 1264.
19 J. A. Zubieta and J. J. Zuckerman, *Prog. Inorg. Chem.*, 1978, **24**, 251.
20 T. J. Marks, *J. Am. Chem. Soc.*, 1971, **93**, 7090.
21 P. Jutzi and W. Steiner, *Chem. Ber.*, 1976, **109**, 3473.
22 W. W. duMont and B. Neudert, *Chem. Ber.*, 1978, **111**, 2267.
23 J. D. Cotton, P. J. Davison, D. E. Goldberg, M. F. Lappert and K. M. Thomas, *J. Chem. Soc., Chem. Commun.*, 1974, **21** 893.
24 J. D. Cotton, P. J. Davidson and M. F. Lappert, *J. Chem. Soc., Dalton Trans.*, 1976, 2275.
25 J. D. Cotton, P. J. Davidson, J. D. Donadlson, M. F. Lappert and J. Silver, *J. Chem. Soc., Dalton Trans.*, 1976, 2286.
26 W. Petz, *Chem. Rev.*, 1986, **86**, 1019.
27 M. F. Lappert and R. S. Rowe, *Coord. Chem. Rev.*, 1990, **100**, 267.
28 M. S. Holt, W. L. Wilson and J. H. Nelsen, *Chem. Rev.*, 1989, **89**, 11.
29 J. J. Schneider, J. Hagen, D. Spickermann, D. Bläser, R. Boese, F. F. d. Biani, F. Laschi and P. Zanello, *Chem.-Eur. J.*, 2000, **6**, 237.
30 M. Weidenbruch, A. Stilter, K. Peters and H. G. v. Schnering, *Z. Anorg. Allg. Chem.*, 1996, **622**, 534.
31 M. Weidenbruch, A. Stilter, K. Peters and H. G. v. Schnering, *Chem. Ber.*, 1996, **129**, 1565.
32 A. Akkari, J. Byrne, J. I. Saur, G. Rima, H. Gornitzka and J. Barrau, *J. Organomet. Chem.*, 2001, **622**, 190.
33 M. Veith, in *Metal Clusters in Chemistry, Molecular Metal Clusters*, eds. P. Braunstein, L. A. Oro and P. R. Raithby, Wiley–VCH Weinheim, New York, 1999, vol. **1**, pp. 73–90.
34 M. Veith, C. Mathur and V. Huch, *Phosphorus, Sulfur Silicon Relat. Elem.*, 1997, **124–125**, 489.
35 M. Veith and O. Recktenwald, *Top. Curr. Chem.*, 1982, **104**, 1.
36 M. Veith, H. Lange, K. Bräuer and R. Bachmann, *J. Organomet. Chem.*, 1981, **216**, 377.
37 M. Weidenbruch, A. Stilter, J. Schlaefke, K. Peters and H. G. v. Schnering, *J. Organomet. Chem.*, 1995, **501**, 67.
38 M. D. Brice and F. A. Cotton, *J. Am. Chem. Soc.*, 1973, **95**, 4529.
39 W. Petz, *J. Organomet. Chem.*, 1979, **165**, 199.
40 A. L. Balch and D. E. Oram, *Organometallics*, 1988, **7**, 155.
41 M. Grenz and W. W. duMont, *J. Organomet. Chem.*, 1983, **241**, C5.
42 P. Braunstein, M. Veith, J. Blin and V. Huch, *Organometallics*, 2001, **20**, 627.
43 A. Tzschach, K. Jurkschat, M. Scheer, J. Meunier-Piret and M. v. Meersche, *J. Organomet. Chem.*, 1983, **259**, 165.
44 K. Jurkschat, A. Tzschach, M. Scheer, J. Meunier-Piret and M. v. Meersche, *J. Organomet. Chem.*, 1988, **349**, 143.
45 H. P. Abicht, K. Jurkschat, A. Tzschach, K. Peters, E. M. Peters and H. G. v. Schnering, *J. Organomet. Chem.*, 1987, **326**, 357.
46 C. Stader, B. Wrackmeyer and D. Schlosser, *Z. Naturforsch., B: Chem. Sci.*, 1988, **43**, 707.
47 I. Mijatovic, G. Kickelbick, M. Puchberger and U. Schubert, *New J. Chem.*, 2003, **27**, 3.
48 J. A. Meese-Marktscheffel, R. E. Cramer and J. W. Gilje, *Polyhedron*, 1994, **13**, 1045.
49 W. Clegg, R. J. Errington, P. Kraxner and C. Redshaw, *J. Chem. Soc., Dalton Trans.*, 1992, 1431.
50 G. A. Sigel, R. A. Bartlett, D. Decker, M. M. Olmstead and P. P. Power, *Inorg. Chem.*, 1987, **26**, 1773.
51 T. J. Boyle, T. M. Alam, M. A. Rodriguez and C. A. Zechmann, *Inorg. Chem.*, 2002, **41**, 2574.
52 (*a*) W. Strohmeier, *Angew. Chem.*, 1964, **76**, 873; (*b*) W. Strohmeier, *Angew. Chem., Int. Ed. Engl.*, 1964, **3**, 730.
53 T. Fjeldberg, P. B. Hitchock, M. F. Lappert, S. J. Smith and A. J. Thorne, *J. Chem. Soc., Chem. Commun.*, 1985, **14**, 939.
54 M. Veith, C. Mathur and V. Huch, *J. Chem. Soc., Dalton Trans.*, 1997, **6**, 995.
55 M. J. McGeary, K. Folting and K. G. Caulton, *Inorg. Chem.*, 1989, **28**, 4051.
56 B. G. McBurnett and A. H. Cowley, *Chem. Commun.*, 1999, 17.
57 B. Schiemenz, B. Antelmann, G. Huttner and L. Zsolnai, *Z. Anorg. Allg. Chem.*, 1994, **620**, 1760.
58 (*a*) P. Kircher, G. Huttner, L. Zsolnai and A. Driess, *Angew. Chem.*, 1998, **110**, 1756; (*b*) P. Kircher, G. Huttner, L. Zsolnai and A. Driess, *Angew. Chem. Int. Ed.*, 1998, **37**, 1666.
59 P. Kircher, G. Huttner, K. Heinze, B. Schiemenz, L. Zsolnai, M. Büchner and A. Driess, *Eur. J. Inorg. Chem.*, 1998, 703.
60 J. T. B. H. Jastrzebski, P. A. van der Schaaf, J. Boersma, G. v. Koten, D. Heijdenrijk, K. Goubitz and D. J. A. De Ridder, *J. Organomet. Chem.*, 1989, **367**, 55.
61 F.-W. Grevels, J. Jacke, W. E. Klotzbucher, F. Mark, V. Skibbe, K. Schaffner, K. Angermund, C. Kruger, C. W. Lehmann and S. Ozkar, *Organometallics*, 1999, **18**, 3278.
62 F. Heinemann, H. Schmidt, K. Peters and D. Thiery, *Z. Kristallogr.*, 1992, **198**, 123.
63 A. Whitaker and J. W. Jeffery, *Acta Crystallogr.*, 1967, **B23**, 977.
64 M. Landman, H. Gorls and S. Lotz, *Eur. J. Inorg. Chem.*, 2001, 233.
65 A. Jost, B. Rees and W. B. Yelon, *Acta Crystallogr.*, 1975, **B31**, 2649.
66 B. Rees and A. Mitschler, *J. Am. Chem. Soc.*, 1976, **98**, 7918.
67 J. E. Huheey, E. A. Keiter and R. L. Keiter, *Inorganic Chemistry: Principles of Structure and Reactivity*, Longman, 4th edn. 1993, p. 428.
68 R. K. Hocking and T. W. Hambley, *Chem. Commun.*, 2003, 1516.
69 M. DiVaira, M. P. Ehses, P. Stoppioni and M. Peruzzini, *Inorg. Chem.*, 2000, **39**, 2199.
70 P. Kircher, G. Huttner, K. Heinze and L. Zsolnai, *Eur. J. Inorg. Chem.*, 1998, 1057.
71 J. G. Verkade, *Coord. Chem. Rev.*, 1972, **9**, 1.
72 *Multinuclear NMR*, ed. J. Mason, Plenum Press, New York, 1987, p. 75.
73 W. W. duMont and H. J. Kroth, *Z. Naturforsch., B: Anorg. Chem. Org. Chem.*, 1980, **35**, 700.
74 (*a*) O. J. Scherer, M. Ehses and G. Wolmershäuser, *Angew. Chem.*, 1998, **110**, 530; (*b*) O. J. Scherer, M. Ehses and G. Wolmershäuser, *Angew. Chem., Int. Ed. Engl.*, 1998, **37**, 507.
75 D. Agustin, G. Rima, H. Gornitzka and J. Barrau, *Eur. J. Inorg. Chem.*, 2000, 693.
76 M. Mehring, C. Löw, M. Schürmann, F. Uhlig, K. Jurkschat and B. Mahieu, *Organometallics*, 2000, **19**, 4613.
77 K. Jurkschat, H.-P. Abicht, A. Tzschach and B. Mahieu, *J. Organomet. Chem.*, 1986, **309**, C47.
78 H. Nakazawa, M. Kishishita, T. Ishiyama, T. Mizuta and K. Miyoshi, *J. Organomet. Chem.*, 2001, **617/618**, 453.
79 R. Xi and L. R. Sita, *Inorg. Chim. Acta*, 1998, **270**, 118.

80 M. Hesse, H. Meier and B. Zeeh, *Spektroskopische Methoden in der organischen Chemie*, Georg Thieme Verlag, Stuttgart, New York, 4th edn., 1991, p. 139.
81 M. Ehses, M. Veith, M. Zimmer and M. Burkhart, 2005, in preparation.
82 T. Athar, B. Bohra and R. C. Mehrotra, *Synth. React. Inorg. Met.-Org. Chem.*, 1989, **19**, 195.
83 R. M. Whittal, G. Ferguson, J. F. Gallagher and W. E. Piers, *J. Am. Chem. Soc.*, 1991, **113**, 9867.
84 H. Nakazawa, Y. Yamaguchi and K. Miyoshi, *Organometallics*, 1996, **15**, 1337.
85 M. Knorr, E. Hallauer, V. Huch, M. Veith and P. Braunstein, *Organometallics*, 1996, **15**, 3868.
86 J. R. Koe, H. Tobita, T. Suzuki and H. Ogino, *Organometallics*, 1992, **11**, 150.
87 K. E. Lee, A. M. Arif and J. A. Gladysz, *Organometallics*, 1991, **10**, 751.
88 (*a*) M. Veith and K. Kunze, *Angew. Chem.*, 1991, **103**, 92; (*b*) M. Veith and K. Kunze, *Angew. Chem., Int. Ed. Engl.*, 1991, **30**, 95.
89 M. Veith, D. Käfer, J. Koch, P. May, L. Stahl and V. Huch, *Chem. Ber.*, 1992, **125**, 1033.